EXPERIMENTAL STUDIES ON THE FIRE BEHAVIOUR OF HIGH PERFORMANCE CONCRETE THIN PLATES

EXPERIMENTAL STUDIES ON THE FIRE BEHAVIOUR OF HIGH PERFORMANCE CONCRETE THIN PLATES

Thomas Hulin[*,1], Cristian Maluk[2], Luke Bisby[2], Kamil Hodicky[1], Jacob W. Schmidt[1], Henrik Stang[1]

[1] Department of Civil Engineering, Technical University of Denmark (DTU), Building 118, Brovej, 2800 Kgs. Lyngby, Denmark

[2] BRE Centre for Fire Safety Engineering, School of Engineering, The University of Edinburgh, King's Buildings, Mayfield Road, Edinburgh, EH9 3JL, UK

Keywords: High-performance concrete, Heat-induced concrete spalling, Thin plates, Testing

Abstract

In recent decades, the use of structural High Performance Concrete (HPC) sandwich panels made with thin plates has increased as a response to modern environmental challenges. Fire endurance is a requirement in structural HPC elements, as for most structural elements. This paper presents experimental investigations on the fire behaviour of HPC thin plates (20 or 30 mm thick) being used in lightweight structural sandwich elements. Tests were undertaken using a standard testing furnace and a novel Heat-Transfer Rate Inducing System (H-TRIS), recently developed at the University of Edinburgh. The parametric assessment of the specimen performance included: thickness of the specimen, testing apparatus, and concrete mix (both with and without polypropylene fibres). The results verified the ability of H-TRIS to impose an equivalent thermal boundary condition to that imposed during a standard furnace test, with good repeatability, and at comparatively low economic and temporal costs. The results demonstrated that heat induced concrete spalling occurred 1 to 5 min earlier, and in a more destructive manner, for thinner specimens. An analysis is presented

combining the thermal material degradation, vapour pore pressure, stress concentrations, and thermo-mechanical energy accumulation in the tested specimens. Unexpectedly, spalling at the unexposed surface was observed during two of the tests, suggesting a potentially unusual, unwanted failure mode of very thin-plates during fire. On this basis it is recommended to favour 30 mm thick plates in these applications, since they appear to resist spalling better than those with 20 mm thickness.

1. Introduction

To face current environmental challenges, the construction industry is pursuing new design solutions resulting in reduced material consumption, and improved thermal insulation and durability. This paper presents a study carried out on novel, optimised precast concrete sandwich elements using unusually thin High Performance Concrete (HPC) plates (20-30 mm thick) framing a phenolic foam insulation layer (300 mm thick). Such elements help to address various environmental challenges in the building industry by their superior insulation performance, reduced material consumption, and comparatively low weight. Structural systems based on these elements can also provide optimised load bearing structures with various possibilities of shear transferring mechanisms [**1-4**].

The well-recognised increased tendency of HPC for heat-induced explosive spalling [**5-7**] presents a challenge in applications where fire safety is a design consideration. Heat-induced concrete spalling occurs by a complex mechanism, the precise sources of which remain unknown. A widely presented theory partly explaining spalling relates to the transport and evaporation of free water (or capillary water) within the concrete pore system; on heating this is hypothesised to lead to capillary vapour pressure accumulation due to low permeability and the generation of a moisture clog, resulting in high tensile stresses and eventually triggering the occurrence of spalling [**8-10**]. Spalling is also

generally considered to be at least partly caused by differential thermal stresses arising from non-uniform thermal gradients within a specimen, and in some cases pore pressure is considered more as an initiator [**11**]. Most researchers now agree that spalling is caused by a combination of these (and potentially other) factors.

Numerous studies have been aimed at modelling heat and moisture transport in heated concrete to calculate the variations in pore pressure and thermal stresses, and thus to try to explain concrete spalling [**12-15**]. Recent experimental studies have directly investigated the relevance of accumulated pore pressure on the occurrence of heat-induced spalling [**16-18**]. Surprisingly, some of these studies have concluded that the magnitude of pore pressure remains low relative to the presumed tensile strength of concrete at elevated temperature, and that higher pore pressures have actually been measured in non-spalling concrete specimens in some cases.

The inclusion of polypropylene (PP) fibres in fresh concrete is now a common technique used for reducing the propensity of concrete for heat-induced spalling. Researchers have suggested that PP fibre inclusion positively modifies the transient moisture migration and/or evaporation processes within concrete during heating [**19, 20**]. Their precise mode of action remains unclear, although at least three potential mechanisms have been proposed.

A first widely used theory, the discontinuous reservoir approach [**21, 22**], states that rapid volumetric changes of the PP fibres during heating result in micro-cracking in the concrete matrix surrounding the fibres, thus creating discrete reservoirs which enhance moisture migration within concrete. Even at ambient temperature, PP fibres promote the creation of discrete reservoirs of air (air entrainment) in the concrete pore structure, resulting in increased permeability [**23**].

Alternatively, Khoury [**24**] has suggested that PP fibres form continuous channels within the concrete during heating, created by the loosening of the boundary layer between concrete and fibres

due to their poor interfacial adhesion and the hydrophobic nature of PP. This phenomenon, named Pressure-Induced Tangential Space (PITS), may allow vapour flow in the channels and enhance moisture migration within concrete. Experiments by Knack [**25**] further suggest that softened fibres are pushed within their channels by the building pore pressure. The process efficiency depends on the PP viscosity, where lower viscosities perform better. Bošnjak et al. [**26**] have presented similar conclusions.

The most widely quoted mechanism suggests the formation of an interconnected network of vacated channels left by melted PP fibres during heating [**27-29**]. This would enhance moisture transport; however there is little evidence for it, particularly as experiments show that PP fibres play a role before their glass transition temperature is reached [**25**].

Existing theories describing the effectiveness of PP fibres are influenced by the properties of the polymeric material, mainly its viscosity, melting point, thermal expansion, and adhesion to the surrounding concrete [**21, 22, 24-29**].

Concrete exposed to high temperatures undergoes material degradation resulting in reduced compressive and tensile strength, and elastic modulus [**9, 30-34**]. Experimental studies have shown that ordinary concrete remains largely unaffected by temperatures up to about 300 °C [**35**] whereas the strength of HPC may reduce by 30% at the same temperature [**36**]. Recent results from Behnood and Gandehari [**36**], on HPC including 10% of cement replacement by silica fume, showed a reduction of splitting tensile strength of 15% at 200 °C and 30% at 300 °C.

Since research has shown that temperature gradients and pore pressure both influence heat-induced concrete spalling, in-depth measurements of both have been made during testing [**10, 11, 17, 27**]. Historically, the potential occurrence of heat-induced spalling has mainly been considered for thick walled concrete structures such as tunnel lining segments or nuclear reactor containment vessels.

Current spalling theories have thus been formulated on the basis of tests on comparatively thick elements. Most tests have involved concrete cylinders, columns, beams, or cubes of minimum dimensions more than 100 mm, with initial heat-induced spalling usually occurring in the first 20 mm [**27, 30, 37-39**]. This corresponds to the full thickness of the thin HPC plates considered in this study for application to optimised foam core sandwich panels, which according to available spalling theories should be expected to be less prone to spalling. Moreover, prior research has typically been performed in standard fire testing furnaces [**40**], this being expensive and time-consuming.

This paper presents novel experiments aimed at gathering initial data on the behaviour of very thin HPC plates during fire, to understand the influence, if any, of thickness (20 versus 30 mm) and PP fibre inclusion, with a view to supporting the development of fire-rated load-bearing sandwich panel elements. Both standard furnace tests and a new test method named the Heat-Transfer Rate Inducing System (H-TRIS) [**41**] have been used. The behaviour of the specimens and the influence of PP fibres are discussed in light of the existing spalling theories, and new potential insights are presented.

2. Experimental work

2.1 Concrete composition

The testing programme was conducted using the same basic HPC mix for all specimens. The mix was designed to yield a compressive strength of 90 MPa at 28 days. Due to the slenderness of the concrete elements, granite aggregate with a maximum size of 10 mm was used. For some specimens circular cross-section PP fibres (Ø 18 μm, length 6 mm) were included in the mix. **Table 1** shows the composition of the HPC mix. All specimens were de-moulded 24 h after casting, sealed in airtight plastic sheets, and maintained at ambient temperature to cure for 28 days. The average 28 day compressive strength was measured as 89 MPa based on a set of 6 cubic specimens (40×40×40

115 mm^3); a tensile strength of 6 MPa was determined by wedge splitting tests and inverse analysis. The
116 initial moisture content (**Table 2**) was assessed by mass loss dehydration at 105 °C. Specimens
117 were weighed every two days and moisture content was calculated as $w=100(m_i-m_t)/m_t$ where w is
118 the moisture content, m_i is the initial mass of the element and m_t is the mass of the element at a
119 given time. The final value was assumed to be reached when two consecutive measurements
120 differed by less than 0.01%.

121 ***2.2 Testing apparatus***

122 ***2.2.1 Furnace tests***

123 The furnace tests were performed at the Danish Fire and Security Institute (DBI) in a medium-scale
124 horizontal furnace (with 1460×1460×1500 mm^3 inner dimensions) with brick floor lining and
125 ceramic fibre walls. Four standard plate thermometers, located 200 mm below the test specimens,
126 controlled the furnace temperature, according to the EN1363-1 standard [**42**]. The furnace
127 temperature followed the standard cellulosic time-temperature curve prescribed in ISO 834 [**43**].

128 The test specimens were placed horizontally, unloaded, on a 100 mm thick concrete supporting
129 frame which also acted as a lid on top of the furnace. The supporting frame incorporated four square
130 holes each presenting a 500×500 mm^2 opening to the furnace. A 15 mm thick layer of Rockwool
131 mineral wool provided flat supports for the test specimens which were exposed to fire on one
132 surface only; unexposed surfaces were exposed to ambient conditions within the laboratory.

133 ***2.2.2 H-TRIS tests***

134 H-TRIS is a novel test method and apparatus that has recently been developed at The University of
135 Edinburgh, and was used in the current project [**44**]. H-TRIS directly controls the time-history of
136 incident radiant heat flux at the exposed surface of a test specimen. H-TRIS uses a mobile array of

propane-fired radiant panels, along with a mechanical linear motion system programmed to actively control the relative position between the radiant panels and the exposed surface of the test specimen (**Figure 1**), and hence to control the time history of incident radiant heat flux. The applied time histories for both furnace and H-TRIS are shown in **Figure 2**, along with actual values from the tests. The agreement between the curves is satisfactory given typical variations in thermal exposures achieved both within and between standard fire testing furnaces.

Although the time history of incident radiant heat flux at the target exposed surface of the test specimen ($\dot{q}''_{inc}$) is the control variable in the H-TRIS testing method, the net heat flux at the exposed surface of the test specimen ($\dot{q}''_{abs}$) can be approximated considering heat losses ($\dot{q}''_{losses}$) at the exposed surface using Eq. 1 and Eq. 2.

$$\dot{q}''_{abs} = \dot{q}''_{inc} - \dot{q}''_{losses} \quad (1)$$

with

$$\dot{q}''_{losses} = h_c(T_S - T_{amb}) + \varepsilon_S \sigma T_S^4 \quad (2)$$

where h_c is the convective heat transfer coefficient; T_s is the temperature of the exposed surface of the specimen; T_{amb} is the ambient temperature; ε_s is the surface emissivity of concrete; and σ is the Stefan-Boltzmann constant. T_s can be calculated from simple heat transfer models. Constant or temperature dependent values may be considered for h_c and ε_s at the exposed surface of the test specimen [**45, 46**].

Using the H-TRIS test method and apparatus, virtually any time history of incident radiant heat flux can be imposed on a test specimen; in practice this is limited only by the range of incident radiant heat fluxes that can be achieved, which in turn is defined by the size and type of radiant panels used

158 and the minimum possible distance between the radiant panels and the exposed surface of the test
159 specimen [**41**].

160 For the current study, H-TRIS was programed to impose a time history of incident radiant heat flux
161 which yielded an equivalent time history of in-depth thermal gradients to those experienced by
162 identical concrete plates tested in the DBI furnace (described above). The net heat flux at the
163 exposed surface of concrete specimens during furnace tests was calculated from in-depth
164 temperature distribution measurements obtained during the furnace tests, and by application of an
165 inverse heat conduction model (described in detail elsewhere [**44**]).

166 ***2.3 Test specimens and recordings***

167 Through thickness temperatures were recorded in the present tests using standard type K
168 thermocouples, with a precision of ±2.5 °C. Time-to-spalling was also recorded. Existing pore
169 pressure sensors are too large compared to thickness of the specimen to allow undisturbed
170 measurements of pore pressure within the HPC plates used in the current study. For example, Kalifa
171 et al. [**27**] noted that they could not embed pressure sensors closer than 10mm from the surface of
172 their test specimens.

173 A total of 12 specimens were prepared, 4 for furnace tests and 8 for H-TRIS tests (see **Table 2**).
174 Thermocouples were placed at ¼, ½ and ¾ of the depth of test specimens during casting. Additional
175 thermocouples were used during testing to record the surface temperatures on the unexposed faces
176 of the HPC plates. All specimens were exposed to heating on their cast face.

177 Furnace test specimens were 540×540 mm^2 plates with a thickness of 20 or 30 mm. Thermocouples
178 inside the specimens were placed at each depth in triplicate (see **Figure 3a**). At the unexposed
179 surface, four coin thermocouples recorded the surface temperatures. All specimens used the same
180 HPC mix.

Specimens tested using H-TRIS were 540×200 mm^2 plates, again with a thickness of 20 or 30 mm. Thermocouples were placed at equivalent depths (with only one at each depth) to those defined for specimens tested using the furnace (**Figure 3b**), and an additional thermocouple was placed on the unexposed surface. The specific concrete mix used for each specimen is indicated in **Table 2**. During casting, PP fibres were added in the dry mix to ensure the maximum homogeneity in their dispersion. Dry mixing lasted for 7 min before water and superplasticiser were added to achieve the required workability.

3. Experimental results

When describing types of heat induced spalling, three terms are employed; these range from a lower to a higher level of damage. The term "flaking" is used to describe the loss of a small, thin layer of concrete without breakage of the specimen and is the lowest level of damage (aside from no spalling whatsoever). The term "fracture" describes cases in which the specimen broke into pieces as a result of spalling. The term "destruction" indicates a sudden and highly explosive spalling event, such that only small debris remained after testing.

For each specimen and each location an average temperature is given; this is calculated as the average of the temperature values recorded at each depth (for specimens with multiple thermocouples at each depth) and at the unexposed surface.

3.1 Furnace tests

Heat induced spalling was observed for all specimens tested in the furnace, at both 20 mm and 30 mm thicknesses. Specimens spalled to destruction by violent and explosive spalling. **Table 2** shows an overview of the test data for moisture content, time-to-spalling, and spalling type.

202 **Table 2** shows that 20 mm thick specimens spalled earlier than the 30 mm thick specimens. The
203 first specimen spalled at 9:40 min (F-20.1) and the last at 15:20 min (F-30.1). No evidence of
204 surface flaking was observed prior to explosive spalling; each specimen experienced only one
205 spalling event leading to sudden and total breakage.

206 Interestingly, the highest initial moisture content of 4.82% (see **Table 2**) was measured in Specimen
207 F-30.1, which spalled latest. However there is little variation in the moisture contents from
208 specimen to specimen, so this may not be significant.

209 The furnace temperature recordings (**Figure 4**) show reasonable consistency for the 20 mm thick
210 specimens, despite the minor moisture content differences between them. The evaporation plateau
211 of water condensing on the unexposed surface is well marked in the data for the thermocouple
212 readings at the unexposed faces. Considerable differences can be observed in temperature
213 recordings for 30 mm thick specimens. For instance, Specimen F-30.1 displayed lower temperatures
214 than F-30.2, and spalled later. The temperature increase in F-30.1 appears less rapid, particularly on
215 the unexposed face. For both 20 mm and 30 mm thick specimens, no obvious plateau corresponding
216 to release of chemically bound water was visible. After 100 s, the temperature within the specimens
217 evolved almost linearly.

218 **Figure 5** shows temperatures recorded at 15 mm in all specimens. As expected, at any given instant
219 in time, the 20 mm thick specimens were hotter than the 30 mm thick specimens; therefore any
220 point between the exposed surface and a depth of 15 mm was hotter in the 20 mm thick specimens,
221 including the exposed surface. As shown in **Figure 4**, at the moment of spalling the temperatures
222 recorded by the thermocouples located closest to the exposed surface were similar (293-297 °C) for
223 the 20 mm thick specimens. For 30 mm thick specimens it was found that F-30.2 spalled when the

224 temperature close to the exposed surface was 261 °C. Generally speaking, at the moment of spalling
225 for a given specimen, the specimen with the hottest bottom surface spalled first.

226 ***3.2 H-TRIS tests***

227 As for the testing in the furnace, heat induced spalling was observed for all specimens tested in H-
228 TRIS. Spalling patterns are shown in **Figure 6**. The 30 mm specimens spalled with light flaking of
229 surface concrete, while 20 mm specimens experienced fracture, except for H-20.1 which showed
230 only flaking of surface concrete. Spalling in 20 mm thick specimens resulted in more extreme
231 damage. The specimens made with the HPC mix containing PP fibres experienced flaking and
232 fracture (H-20PP.1) or complete destruction (H-20PP.2). Results for moisture content, time-to-
233 spalling and spalling type are given in **Table 2**.

234 The observation that in furnace tests the 20 mm thick specimens spalled before the 30 mm thick
235 specimens was corroborated in the H-TRIS tests for specimens without PP fibres. The first of these
236 specimens spalled at 8:36 min (H-20.3) and the last at 11:39 min (H-30.1). Tests were halted
237 immediately after the first spalling event in all cases. As for the furnace tests, no evidence of the
238 influence of moisture content could be clearly isolated. The H-TRIS specimens generally had
239 slightly lower moisture contents than furnace specimens, however this is not thought to be
240 significant.

241 The scatter in the temperature recordings for H-TRIS specimens without PP fibres (**Figure 4**) is
242 larger for the 20 mm thick specimens than for the 30 mm thick specimens. Overall the results are
243 reasonably consistent for both thicknesses and show good repeatability. No evaporation or water
244 release plateau is visible in H-TRIS curves, as was the case for furnace tests. The recordings on the
245 unexposed surface display no evaporation plateau. Indeed no condensation water was visible on the
246 unexposed surface of these specimens, which may be due to their vertical position preventing the

247 gathering of condensation water on the unexposed surface. The same almost linear temperature
248 evolution as in furnace tests can be noted, especially at the unexposed surfaces.

249 The moment of spalling occurred when temperature close to the exposed surface was in the range of
250 249-280 °C (see **Figure 4**). These temperatures are generally lower than those recorded during the
251 furnace tests. Temperatures recorded at a depth of 15 mm in all specimens show that the 20 mm
252 thick specimens were hotter than the 30 mm thick specimens at any given instant (**Figure 5**). At the
253 moment of spalling for a given specimen, the specimen with the highest exposed surface
254 temperature spalled first. Furthermore, in the H-TRIS tests on 20 mm thick specimens it was
255 usually the specimen with the highest average temperature which spalled first; this was not the case
256 for the 30 mm thick specimens in which the average temperatures at the moment of spalling
257 differed widely between specimens.

258 Specimens with PP fibres, all of which were 20 mm thick, generally spalled between 11 and 18 min,
259 while 20 mm thick specimens without PP fibres spalled earlier (between 8 and 10 min). The
260 fracture pattern of spalling also differed when PP fibres were present. For H-20PP.1, flaking of
261 concrete layers occurred on the unexposed surface of the specimen, instantly followed by fracture
262 through the thickness (**Figure 6**). Specimen H-20PP.2 spalled in a violent explosion and much
263 sooner than H-20PP.1. Some debris showed the typical thin circular peels from surface flaking, the
264 outer surfaces of which were either the exposed or unexposed side (**Figure 7**). This suggests that
265 the specimen spalled from both surfaces. It was not possible to tell which surface spalled first due to
266 the violence of the spalling event.

267 The temperature recordings in specimens with PP fibres are shown in **Figure 8**. The difference
268 between the temperatures recorded at 5 and 10 mm depths below the exposed surface was greater
269 than that in specimens without PP fibres (**Figure 8 right**). Specimen H-20PP.2 showed a hotter

exposed surface than H-20PP.1. At the moment of spalling, the unexposed surface of H-20PP.2 displayed the same temperature as the thermocouple located at a depth of 15 mm from the exposed surface. Overall, specimen H-20PP.2 appeared much hotter than H-20PP.1.

3.3 Sensitivity analysis for temperature recordings

A sensitivity analysis on the test data has been performed to estimate the degree of confidence in the position of the thermocouples; this uses a simple heat transfer model which estimates the temperatures with time at a distance of 1 mm on either side of the intended thermocouple location. **Figure 9** shows the resulting predicted error for both 20 mm and 30 mm thick specimens. The impact of a thermocouple deviating from its intended position by ± 1 mm during casting, for the worst case of a 20 mm thick specimen, at earlier exposure time, and closer to the exposed surface, is an error of ± 8%. At the moment of spalling, the largest uncertainty is ± 5%, again close to the exposed surface. Since temperatures recorded at a given time and depth vary between specimens by the estimated maximum error (**see Figure 4, Figure 5 and Figure 8**), the test results are deemed as acceptable in supporting the observations and conclusions presented herein. However, these potential variations could partly explain the large differences observed in average temperatures between specimens of the same thickness at the same exposure time.

4. Discussion and analysis

4.1 Specimen thickness

The data presented in this paper suggest a tendency for 20 mm thick specimens to spall sooner than 30 mm specimens. This observation is counter-intuitive when considering other published material, particularly as regards differential thermal stress development. Usually heat-induced spalling occurs within the first 20 mm of a concrete specimen's thickness [**10**], suggesting that a minimum amount

292 of water is necessary to build up a sufficient moisture clog and pore pressure and trigger spalling
293 (assuming pore pressure spalling as a dominant mechanism). Using this reasoning it is not obvious
294 that a 20 mm specimen would spall. Furthermore, the thinner concrete sections are more able to
295 undergo thermal bowing during heating, an effect that would to some extent relieve differential
296 thermal stresses and cold restraint from the cooler unexposed surface of the specimens; thus also
297 promoting a lower propensity for spalling.

298 However, due to their smaller thickness, the thinner 20 mm thick plates heat up faster than the 30
299 mm thick specimens (**Figure 5**). This results in the 20 mm thick specimens being overall hotter than
300 the 30 mm thick specimens at a given instant in time, particularly towards the exposed surface.
301 Temperatures therefore increase more rapidly through the thickness of 20 mm specimens. This has
302 two main consequences.

303 The first consequence concerns temperature-induced material degradation, which will be greater for
304 specimens reaching higher temperatures, as indicated by Behnood and Ghandehari [**36**] who
305 considered concrete material degradation with temperature. The ability of the thinner profiles to
306 sustain high stresses is therefore reduced and the likelihood of earlier spalling increased. This is
307 supported by the observation that at a given time, the specimen with the highest exposed surface
308 temperature spalled first.

309 However, it was not always the specimen with the highest average temperature which spalled first
310 at a given time. This suggests that a high degree of localised thermal degradation may be more
311 critical than an overall more degraded specimen. This could partially explain the violence and time-
312 to-spall in the H-20PP.2 spalling event at about 11 minutes. Close to the exposed surface, specimen
313 H-20PP.2 displayed much higher temperatures than H-20PP.1, thus showing a larger localised
314 thermal degradation and gradient.

315 Considering this observation in light of damage mechanics provides additional insights. In damage
316 mechanics theory [**47, 48**], when a material becomes degraded (by mechanical or thermal loading)
317 the resisting area, also known as the effective area, reduces with growing damage [**49, 50**]. Since
318 the loads stay the same, stresses on plain material (effective stresses) artificially rise. The more
319 degraded the material, the more rapidly it will continue to degrade. The material at macro-scale will
320 experience a reduction of elastic modulus with heating. This should lead to comparatively smaller
321 nominal stresses (stresses applied over the entire specimen, including both the resisting area and
322 damaged area). The effective stresses would therefore rise because of the low effective area.
323 Additional stress concentrations could be expected from this phenomenon, by force application on
324 smaller areas, and a more tortuous geometry created by newly formed discrete cracks.

325 The second consequence concerns the pore pressure build-up. This comes from free water
326 evaporation, and also from the release and evaporation of chemically-bound water. This water
327 contributes to a rise in pore pressure, which is thought to be sufficient to trigger spalling under the
328 right conditions [**10**]. A hotter specimen would have more water released and evaporated more
329 quickly, leading to higher pressures [**51**].

330 Those two consequences could explain the above-mentioned tendency of thinner specimens to spall
331 sooner; a behaviour that appears in the particularly thin plates tested herein, and which is opposite
332 to what has been observed experimentally on thicker concrete slabs (say 200 mm thick) [**18**].

333 Finally, it is worth considering also that spalling represents a release of energy accumulated by
334 heating in the specimen. Both the mass and the strength of a structure define its ability to resist an
335 energy release. A thicker, more massive structure needs more energy than a thin structure to
336 experience violent fracture. Similarly a more degraded structure can explode at lower energy levels.
337 The thermal energy absorbed by a specimen can be calculated as the area under the curve of

absorbed heat flux versus time. Time-dependent net heat flux was calculated using Eq. 1 and Eq. 2. The exposed surface temperature was approximated using a simple heat transfer model which uses the recording from the thermocouple located closest to the exposed surface as boundary condition. The integral of the net heat flux curve is taken over the exposure time, and the corresponding energy (scaled down to the exposed area) for each specimen could be calculated. It was found that when specimens spalled, the 30 mm thick specimens had accumulated a maximum of 40 % more energy than the 20 mm thick specimens (3970 kJ and 2820 kJ respectively). Their thickness being 50% larger, it is postulated that they were thus able to sustain a larger accumulated energy before experiencing spalling. Additional research is required to corroborate this possible correlation.

4.2 PP fibres

Specimens made of the mix that incorporated PP fibres were not resistant to spalling, however they generally experienced spalling later than other specimens. It is also noteworthy that when PP fibres were used, spalling occurred either on the unexposed surface only (H-20PP.1) or on both surfaces (H-20PP.2), apparently simultaneously.

In the present study, all specimens were tested in an unloaded (i.e. unrestrained) condition. The furnace test specimens will have experienced some minimal amount of restraint to thermal expansion from the cold concrete frame created on the exposed surface by the supporting mineral wool. The specimens tested using H-TRIS were unrestrained and free to expand. Based on these considerations, the main stresses involved in the spalling process are the pore pressure-induced tensile stresses acting on the porous matrix, and the differential thermal stresses resulting from through-thickness thermal gradients. In a dense matrix composed of micro-scale pores, the effect of local stress concentrations arising from the geometrical configuration of these pores cannot be ignored. In the case of cavities in an infinite body, the stress concentration factor can rise up to 7

according to the shape of the cavities [**52**]. For such a scenario, even low pressures could become an issue and a combination of this factor with tensile strength degradation could lead to spalling. This approach could also explain recent experimental results recording very low pore pressures yet still showing a spalling event, thus reducing the potential role of pore pressure as a spalling trigger [**17, 53**].

Polypropylene fibres for spalling mitigation had a delaying role in the tests presented herein, however they did not prevent spalling. According to the accepted mechanisms of PP fibres action described earlier in this paper, the creation of channels and the fibre softening on heating potentially modify the geometry of the pore structure and increase the water vapour flow. Thus, the stress concentration factor considered earlier would reduce through geometrical changes such as pore widening, and/or the impact of this factor would be indirectly lowered by moisture vapour flowing more easily in the channels and spaces made available by the softening PP fibres; thus limiting moisture vapour accumulation. In both cases, a pore pressure reduction would be observed.

The occurrence of spalling on the unexposed surface in two of the H-TRIS tests was an unexpected behaviour for concrete exposed to high temperatures. To attempt to explain this, a critical zone is defined at a given location through the thickness of the specimen, in which the fracture that manifests as spalling occurs. This zone theoretically corresponds to a high pressure zone, potentially created by a moisture clog resulting from the re-condensation in the pores of moisture vapour in contact with colder zones and leading to an incompressible region [**12**, **53**]. This is presumed to be located some distance away from the exposed surface, since moisture is driven inwards by pressure gradients after the initial evaporation towards heat. The critical zone then moves through the thickness of the specimen with changing conditions of temperature, material degradation, and pore pressure, this movement made possible in part by the PP fibres' action to increase the permeability. In this manner, a new high pressure zone could form farther inside the

specimen and give rise to a first crack. From this crack, the surface experiencing spalling could be defined by the energy considerations described above. If the crack occurs close to the unexposed side, this surface will spall, as seen for H-20PP.1. If the first crack occurs closer to the mid-section however, and the temperature exposure has weakened the cementitious matrix, both the exposed and unexposed surfaces may spall, as seen on H-20PP.2. This idea is supported by the fact that spalling of H-20PP.1 occurred much later than for other specimens, meaning that the critical zone could have migrated further toward the unexposed face.

The major differences of behaviour between H-20PP.1 and H-20PP.2, particularly in terms of time-to-spalling, remain largely unexplained. The specimens were similar and the H-TRIS apparatus was calibrated and operated in the same way. H-20PP.2 displayed much higher measured temperatures, which according to the considerations from Section 4.1 would lead to more degradation and faster pressure build-up. A reasonable explanation for higher and faster temperature build-up has not been found.

The HPC mix with PP fibres contained the current Eurocode recommendation of 2 kg of PP fibres per cubic meter of concrete to mitigate explosive spalling in high strength mixes. This proved insufficient for the mixes tested in the current study. Many material parameters of the PP fibres, including the amount, type, shape, length, diameter, viscosity, or glass transition temperature are thought to affect the performance of PP fibres in heat-induced spalling mitigation; these are not accounted for in the Eurocode guidance. More precise guidelines should therefore be proposed in the Eurocodes, since the current regulations have been proven insufficient to prevent (or even clearly mitigate) spalling for the mixes tested herein.

4.3 Furnace versus H-TRIS testing

407 The major difference between the results of tests carried out in the furnace and with H-TRIS was in
408 the violence of the spalling events. H-TRIS specimens presented flaking of surface layers or
409 specimen breakage, whereas all furnace specimens experienced complete destruction and exploded
410 into many pieces.

411 Furnace specimens laid on mineral wool for insulation from the supporting frame. This support
412 condition created a 2 cm frame of unexposed concrete all around the exposed surface of the
413 specimens. This frame did not heat up directly, whereas the central part of furnace specimens was
414 exposed to heat and experienced thermal expansion. This thermal expansion may have been
415 partially restrained by the unheated perimeter of the specimens, which may have prevented the
416 thermal expansion and induced additional thermal stresses through the plate. The small thickness of
417 the plates potentially limited this restraint; however the cooler 2 cm frame also had its edges
418 exposed to the environment, thus cooling down the sides of the specimen. This could partly explain
419 the difference in violence between the spalling events of the two test apparatus.

420 Heating specimens of identical thickness but different widths requires different amounts of energy,
421 but the energy per kg of concrete used to reach a given temperature remains the same provided that
422 the sample thickness is held constant. Additionally, this can permit self-bowing due to thermal
423 gradients. Therefore no definite conclusion on the influence of the sample width difference between
424 furnace and H-TRIS specimens can be provided.

425 ***4.4 Moisture content***

426 The highest moisture contents were recorded in specimens that experienced spalling later; however
427 all measured moisture content values were reasonably similar (**Table 2**). The moisture content
428 variations between specimens may not have been sufficiently large to explain either the differences
429 in time-to-spalling between specimens or the observation that the 20 mm thick specimens spalled

first. According to the available literature, larger moisture contents should lead to lower recorded temperatures in the specimens since more thermal energy would be consumed during evaporation and transport. This is not seen in the test data presented in **Figure 4**, however this could be a result of mild thermocouple displacement during casting.

5. Conclusion

The experiments carried out in the present study showed that thinner specimens of HPC (counter-intuitively) spalled slightly earlier than thicker ones. Based on the available literature, this behaviour appears to be specific to thin plates. It could possibly be explained by larger thermal material degradation and strength reduction in specimens with thinner sections, which can be expected to heat up faster and overall experience higher temperatures.

Specimens with a thickness of 20 mm broke when spalling due to the thermal energy released at that time, suggesting higher overall spalling risk in their use than 30 mm thick sections. Thicker specimens absorbed higher levels of thermal energy; however their increased thickness was apparently able to withstand this, leading to longer times-to-spalling.

Heating tests on thin HPC specimens with polypropylene fibres suggested that stress concentration factors should be accounted for in the estimation of pore pressure induced tensile stresses. This could explain the observation that the pore pressure values recorded in literature that are low compared to the high temperature tensile strength of HPC may still lead to spalling events. A different possibility for the mode of action for PP fibres is proposed in light of the observations from the tests on thin sections presented herein, combining moisture movement, pore pressures, and thermal material degradation. By softening and/or melting, PP fibres would ease moisture movements in the matrix, possibly transporting water vapour farther into the section. Thermal stresses would then be relaxed by drying and decreased stiffness due to thermal degradation.

Specimens would then spall when pressure-induced and thermal stresses overtake the relaxation and degradation. Eurocode recommendations on the use of PP fibres should be regarded critically, since the recommended 2 kg/m^3 was insufficient to prevent spalling in all cases in the current study.

The comparison between the two test methods verified the ability of H-TRIS to impose an equivalent thermal boundary condition to that imposed during a standard furnace test. This was achieved with good repeatability, and at comparatively low economic and temporal costs.

6. Recommendations for future work

Based on the results obtained, future work should focus on the issues of specimen size, restraint, and inclusion in a sandwich structure. The thin plates presented in this work were tested in an unrestrained and unloaded condition; this represents a first step in the product development process but requires further investigation in real-life configurations, scales, and loading scenarios. Scaling up the plates represents a significant challenge, as walls in real applications can reach sizes up to 3×4 m^2, whereas both test setups presented herein involved much smaller specimens. Similarly, the influence of the elements involved in the sandwich structure must be assessed. Shear connectors and other structural details could be expected to introduce restraint to thermal bowing of the plate. Insulation layers, by preventing cooling on the unexposed side of the exposed plate, can be expected to lead to different in-plane temperature distributions, which could potentially lead to additional or different thermal stresses, with possible consequences for spalling performance in fire.

Acknowledgements

The authors would like to acknowledge the support of the Otto Mønsted and Oticon funds that supported the first author's research visit to the BRE Centre for Fire Safety Engineering at The University of Edinburgh. Special thanks are given to Ieuan Rickard and Dr David Rush for their

475 contributions to the experimental work. The support of Ove Arup and Partners Ltd, the Royal
476 Academy of Engineering, and the Royal Society of Edinburgh are gratefully acknowledged.

477 References

478 [1] Morcous G, Tadros MK, Lafferty M, Gremel D (2010) Optimised NU sandwich panel system
479 for energy efficiency, composite action and production efficiency. In: Proceedings of the 3rd FIB
480 International Congress, Washington D.C., USA, 29 May-2 June.

481 [2] Gara F, Ragni L, Roia D, Dezi L (2012) Experimental tests and numerical modelling of wall
482 sandwich panels. Eng Struct 37:193-204.

483 [3] Hodicky K, Hulin T, Schmidt JW, Stang H (2013) Structural performance of new thin-walled
484 concrete sandwich panel system reinforced with BFRP shear connectors. In: Proceedings of the 4th
485 Asia-Pacific Conference on FRP in Structures, Melbourne, Australia, 11-13 December.

486 [4] Lameiras R, Barros J, Valente IB, Azenha M (2013) Development of sandwich panels
487 combining fibre reinforced concrete layers and fibre reinforced polymer connectors. Part II:
488 Evaluation of mechanical behaviour. Compos Struct 105:446-459.

489 [5] Barber C, Gardiner A, Law M (1994) Structural fire design of the Øresund tunnel. In:
490 Proceedings of the International Conference on Fires in Tunnels, Boras, Sweden, 295-316.

491 [6] Ulm FJ, Acker P, Lévy M (1999) The Chunnel fire II: analysis of concrete damage. J Eng Mech
492 125:283-289.

493 [7] Garlock M, Paya-Zaforteza I, Kodur V, Gu L (2012) Fire hazard in bridges: Review, assessment
494 and repair strategies. Eng Struct 35:89-98.

495 [8] Khoury GA (2000) Effect of fire on concrete and concrete structures. Prog Struct Eng Mater
496 2:429-447.

497 [9] Phan LT, Lawson JR, Davis FL (2001) Effects of elevated temperature exposure on heating
498 characteristics, spalling and residual properties of high performance concrete. Mater Struct 34:83-
499 91.

500 [10] Hertz KD (2003) Limits of spalling of fire-exposed concrete. Fire Saf J 38:103-116

501 [11] Bažant ZP (1997) Analysis of pore pressure, thermal stress and fracture in rapidly heated
502 concrete. In: Proceedings of the International Workshop on Fire Performance of High-Strength
503 Concrete, NIST, Gaithersburg, MD, USA, 13-14 February, 155-164.

504 [12] Bažant ZP, Thonguthai W (1979) Pore pressure in heated concrete walls: theoretical
505 prediction. Mag Concr Res 31:67-76.

[13] Majorana CE, Salomoni V, Schrefler BA (1998) Hygrothermal and mechanical model of concrete at high temperature. Mater Struct 31:378-386.

[14] Gawin D, Pesavento F (2012) An overview of modelling cement based materials at elevated temperatures with mechanics of multi-phase porous media. Fire Technol 48:753-793.

[15] Dwaikat MD, Kodur VKR (2009) Hydrothermal model for predicting fire-induced spalling in concrete structural systems. Fire Saf J. 44:425-434.

[16] Arita K, Harada K, Miyamoto S (2002) Thermal spalling of high performance concrete during fire. In: Proceedings of the 2nd international workshop Structures in Fire, Christchurch, New Zealand, March, 253-271.

[17] Mindeguia JC, Pimienta P, Noumowé A, Kanema M (2010) Temperature, pore pressure and mass variation of concrete subjected to high temperature – Experimental and numerical discussion on spalling risk. Cem Concr Res 40:477-487.

[18] Jansson R, Boström L (2013) Factors influencing fire spalling of self-compacting concrete. Mater Struct 46:1683-1694.

[19] Zeiml M, Leithner D, Lackner R, Mang HA (2006) How do polypropylene fibres improve the spalling behaviour of in-situ concrete? Cem Concr Res 36:929-942.

[20] Liu X, Ye G, De Schutter G, Yuan Y, Taerwe L (2008) On the mechanism of polypropylene fibres in preventing fire spalling in self-compacting and high-performance cement paste. Cem Concr Res 38:487-499.

[21] Smith K, Atkinson TW (2009) Factors to consider in using PP fibres for explosive spalling resistance. In: Proceedings of the 1st International Workshop on Concrete Spalling due to Fire Exposure, Leipzig, Germany, 364-373.

[22] Huismann S, Korzen M, Weise F, Meng B (2011) Concrete spalling due to fire exposure and the influence of polypropylene fibres on microcracking. In: Proceedings of the 2nd International RILEM Workshop on Concrete Spalling due to Fire Exposure, Delft, The Netherlands, 5-7 October, 327-336.

[23] Bayasi Z, Zeng J (1993) Properties of polypropylene fibre reinforced concrete. ACI Mater J 90:605-610.

[24] Khoury GA (2008) Polypropylene fibres in heated concrete. Part 2: pressure relief mechanisms and modelling criteria. Mag Concr Res 60:189-204.

[25] Knack I (2011) The use of PP fibres in tunnel construction to avoid explosive concrete spalling in case of fire. New test results for the clarification of the mode of action. In: Proceedings of the 2nd International RILEM Workshop on Concrete Spalling due to Fire Exposure, Delft, The Netherlands, 5-7 October, 297-307.

[26] Bošnjak J, Ožbolt J, Hahn R (2013) Permeability measurement on high strength concrete without and with polypropylene fibres at elevated temperatures using a new test setup. Cem Concr Res 53:104-111.

[27] Kalifa P, Chéné G, Gallé C (2001) High-temperature behaviour of HPC with polypropylene fibres – From spalling to microstructure. Cem Concr Res 31:1487-1499.

[28] Bentz DP (2000) Fibres, percolation and spalling of high performance concrete. ACI Mater J 97:351-359.

[29] Pistol K, Weise F, Meng B, Schneider U (2011) The mode of action of polypropylene fibres in high performance concrete at high temperatures. In: Proceedings of the 2nd International RILEM Workshop on Concrete Spalling due to Fire Exposure, Delft, The Netherlands, 5-7 October, 289-296.

[30] Li M, Qian CX, Sun W (2004) Mechanical properties of high-strength concrete after fire. Cem Concr Res 34:1001-1005.

[31] Komonen J, Penttala V (2003) Effects of high temperature on the pore structure and strength of plain and polypropylene fibre reinforced cement pastes. Fire Technol 39:23-34.

[32] Chan YN, Luo X, Sun W (2000) Compressive strength and pore structure of high-performance concrete after exposure to high temperature up to 800 °C. Cem Concr Res 30:247-251.

[33] Khaliq W, Kodur V (2011) Thermal and mechanical properties of fibre reinforced high performance self-consolidating concrete at elevated temperatures. Cem Concr Res 41:1112-1122.

[34] Rahim A, Sharma UK, Murugesan K, Sharma A, Arora P (2013) Multi-response optimisation of post-fire residual compressive strength of high performance concrete. Constr Build Mater 38:265-273.

[35] Phan LT, Carino NJ (2003) Code provisions for high strength concrete strength-temperature relationship at elevated temperatures. Mater Struct 36:91-98.

[36] Behnood A, Ghandehari M (2009) Comparison of compressive and splitting tensile strength of high-strength concrete with and without polypropylene fibres heated to high temperatures. Fire Saf J 44:1015-1022.

[37] Noumowe A (2005) Mechanical properties and microstructure of high strength concrete containing polypropylene fibres exposed to temperatures up to 200°C. Cem Concr Res 35:2192-2198.

[38] Peng GF, Yang WW, Zhao J, Liu YF, Bian SH, Zhao LH (2006) Explosive spalling and residual mechanical properties of fibre-toughened high-performance concrete subjected to high temperatures. Cem Concr Res 36:723-727.

573 [39] Noumowe A, Siddique R, Debicki G (2009) Permeability of high-performance concrete
574 subjected to elevated temperature (600°C). Constr Build Mater 23:1855-1861.

575 [40] Sultan MA (2006) Incident heat flux measurements in floor and wall furnaces of different
576 sizes. Fire Mater 30:1-17.

577 [41] Maluk C, Bisby L, Krajcovic M, Torero JL (2015) The Heat-Transfer Rate Inducing System
578 (H-TRIS) test method. Fire Saf J (sent to editor)

579 [42] PrEN 1363-1:1999 Fire resistance tests. General requirements

580 [43] ISO 834:2014 Fire resistance tests.

581 [44] Maluk C (2014) Development and application of a novel test method for studying the fire
582 behaviour of CFRP prestressed concrete structural elements. Ph.D. thesis, University of Edinburgh,
583 UK.

584 [45] PrEN 1992-1-2:2004 Design of concrete structures

585 [46] Incropera FP, DeWitt DP, Bergman TL, Lavine AS (2007) Fundamentals of heat and mass
586 transfer. John Wiley & Sons, New York.

587 [47] Voyiadjis GZ, Kattan PI (2005) Damage mechanics. Taylor & Francis, CRC Press, New York.

588 [48] Krajcinovic D, Fonseka GU (1981) The continuous damage theory of brittle materials – Part 1:
589 General theory. J Appl Mech 48:809-815

590 [49] Chaboche JL (1988) Continuum damage mechanics: Part II – Damage growth, crack initiation,
591 and crack growth. J Appl Mech 55:65-72

592 [50] Lemaitre J (1984) How to use damage mechanics. Nucl Eng Des 80:233-245.

593 [51] Phan LT (2008) Pore pressure and explosive spalling in concrete. Mater Struct 41:1623-1632.

594 [52] Pilkey WD (1997) Peterson's stress concentration factors. John Wiley & Sons, New York.

595 [53] Jansson R, Boström L (2010) The influence of pressure in the pore system on fire spalling of
596 concrete. Fire Technol 46:217-230.

597

598

599

600

601

602 **LIST OF TABLES**

603 Table 1 – Composition of the high performance concrete mixes

Concrete constituents	**HPC**	**HPC PP**
Cement CEM I 52.5 R [kg/m^3]	495	495
Microsilica [kg/m^3]	55	55
Fine aggregates (0-2 mm) [kg/m^3]	782	782
Coarse aggregates (3-10 mm) [kg/m^3]	868	868
Sand/aggregates ratio	0.90	0.90
Water [kg/m^3]	165	165
Water/binder ratio	0.30	0.30
Superplasticiser [kg/m^3]	11	11
Polypropylene fibres (6 mm, Ø18 μm) [kg/m^3]	-	2
$f_{c,28}$ [MPa]	90	90

604

605

606

607

608 Table 2 – Identification of test specimens and test results for all specimens tested in furnace and
609 with H-TRIS

Specimen*	**Test apparatus**	**Concrete mix**	**Thickness [mm]**	**Moisture content [%]**	**Time-to-spalling [mm:ss]**	**Spalling type**
F-20.1	Furnace	HPC	20	4.77	9:40	Destruction
F-20.2				4.54	10:50	Destruction
F-30.1			30	4.82	15:20	Destruction
F-30.2				4.74	10:50	Destruction
H-20.1	H-TRIS		20	3.94	9:15	Light flaking
H-20.2				4.35	9:16	Flaking + fracture
H-20.3				4.35	8:36	Flaking + fracture
H-30.1			30	3.87	11:39	Light flaking
H-30.2				4.52	10:32	Light flaking
H-20PP.1		HPC PP	20	4.21	18:01	Flaking + fracture
H-20PP.2				4.21	11:04	Destruction

* *F or H indicates the test set-up (Furnace or H-TRIS)*
-20 or -30 indicates the thickness of the specimen
PP indicates the use of concrete mix HPC PP including PP fibres
.1 or .2 or .3 indicates repeat test

610

611

612 **LIST OF FIGURES**

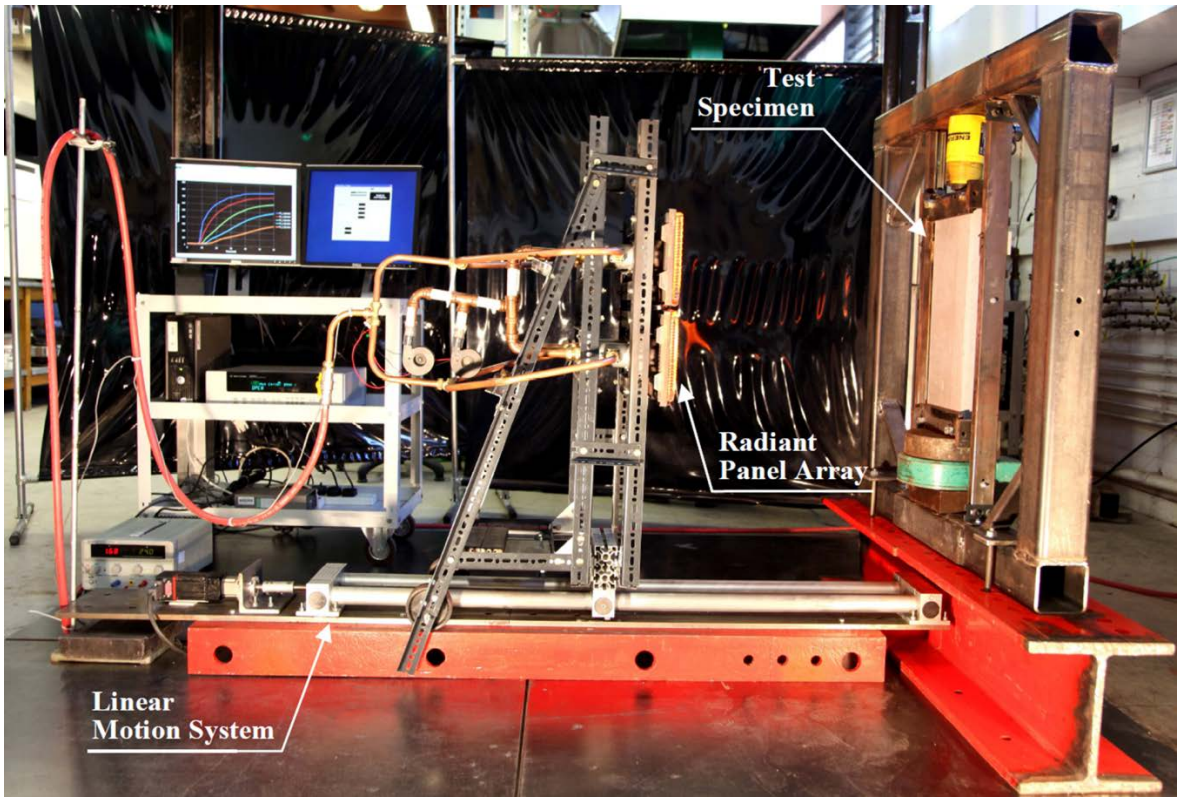

613

614 Figure 1 – Heat-Transfer Rate Inducing System (H-TRIS) Mk I [41]

615

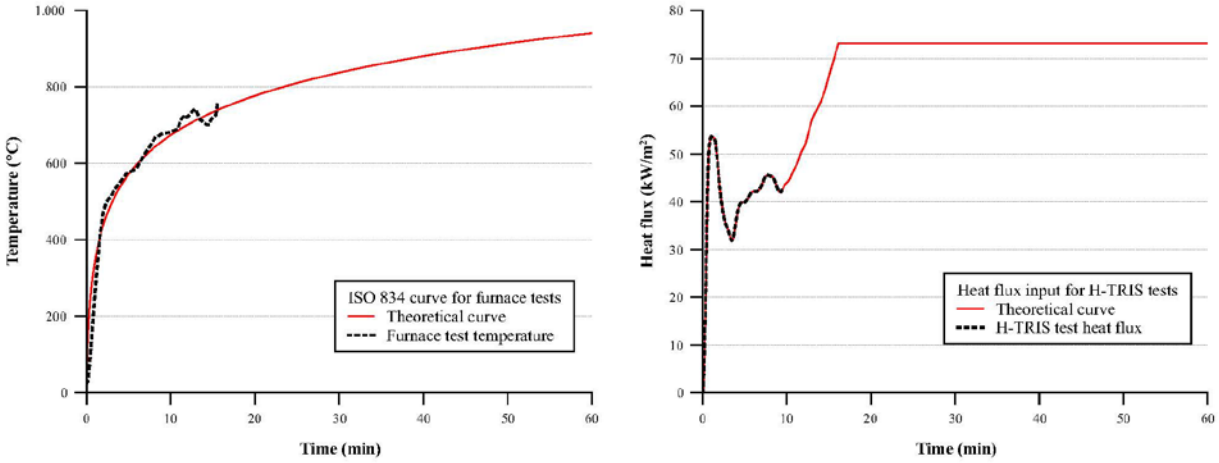

616

617 Figure2 – Time history of temperature imposed during furnace tests (left) and of incident radiant
618 heat flux at exposed surface during tests with H-TRIS tests (right)

619

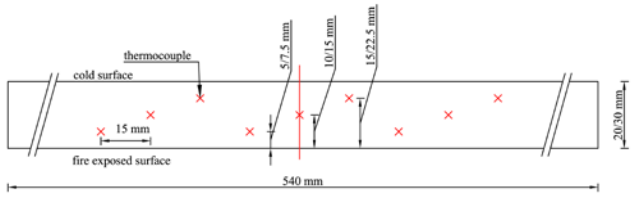

620 a

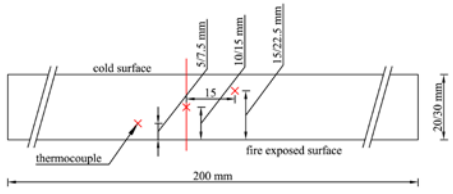

621 b

622 Figure 3 – Cut of the test specimens for furnace tests (a) and H-TRIS tests (b)

623

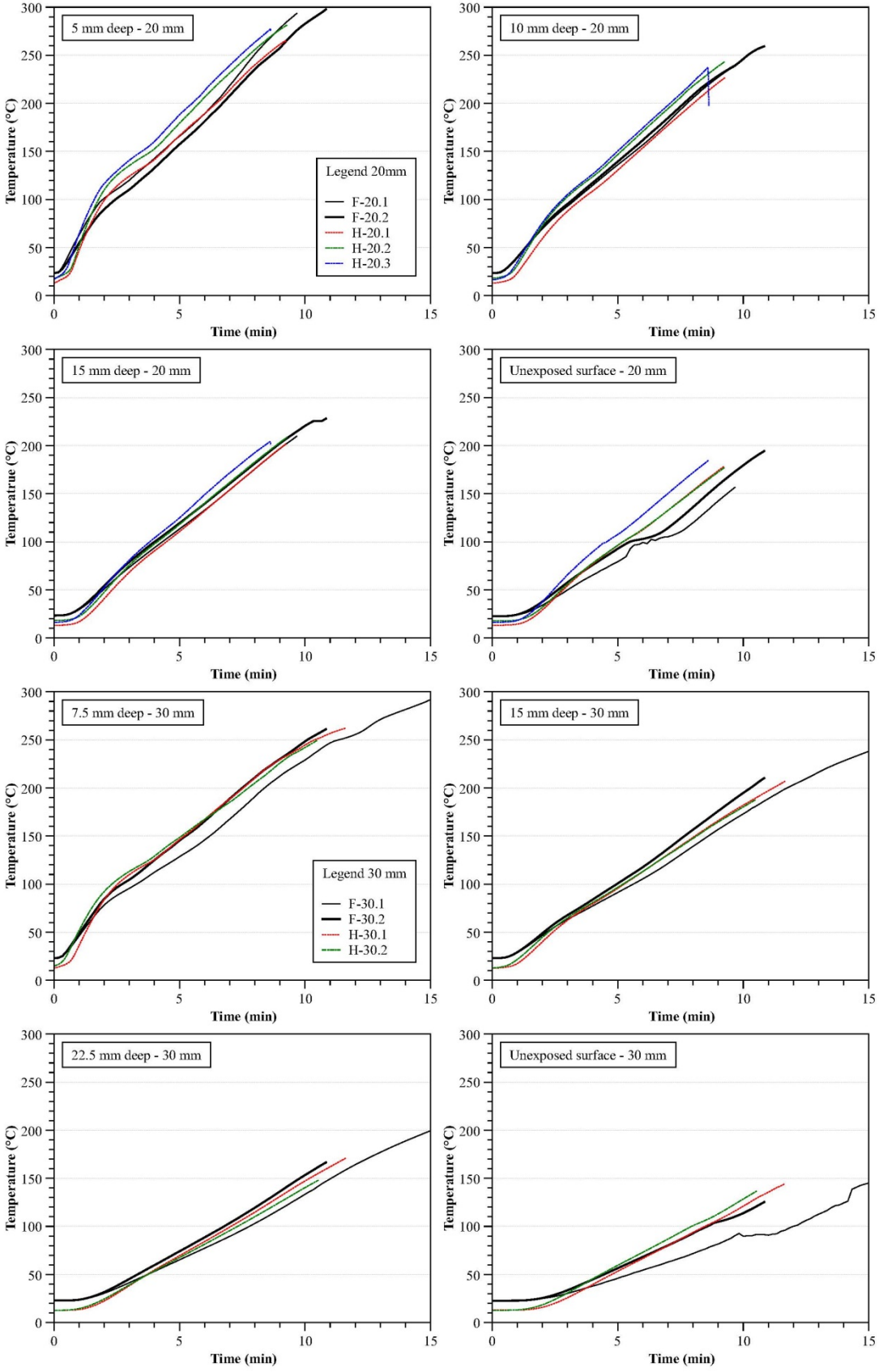

Figure 4 – Temperature recordings for furnace and H-TRIS specimens for HPC without PP fibres

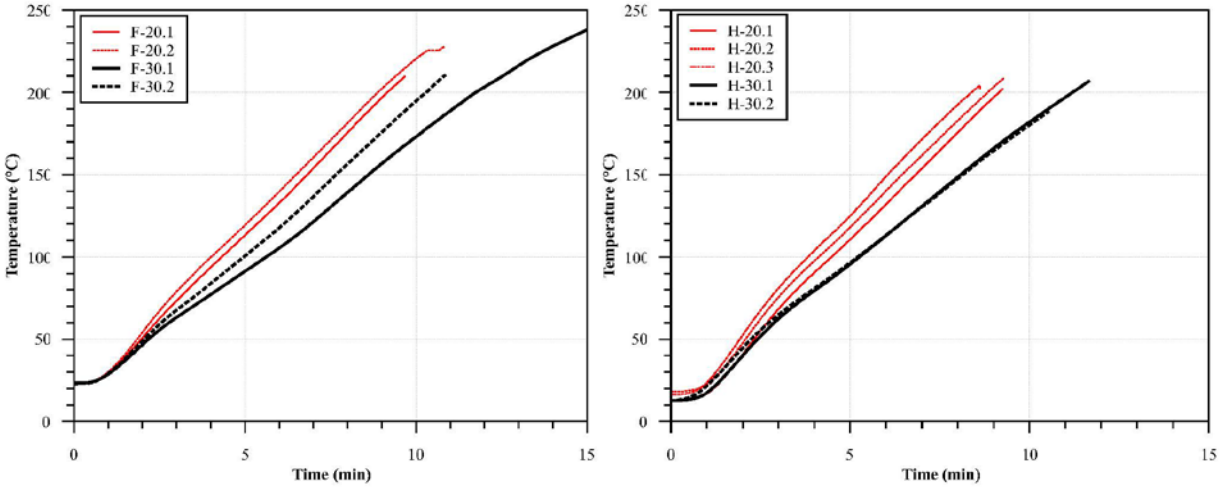

626

627 Figure 5 – Temperature recordings at 15 mm in all specimens for furnace (left) and H-TRIS (right)

628

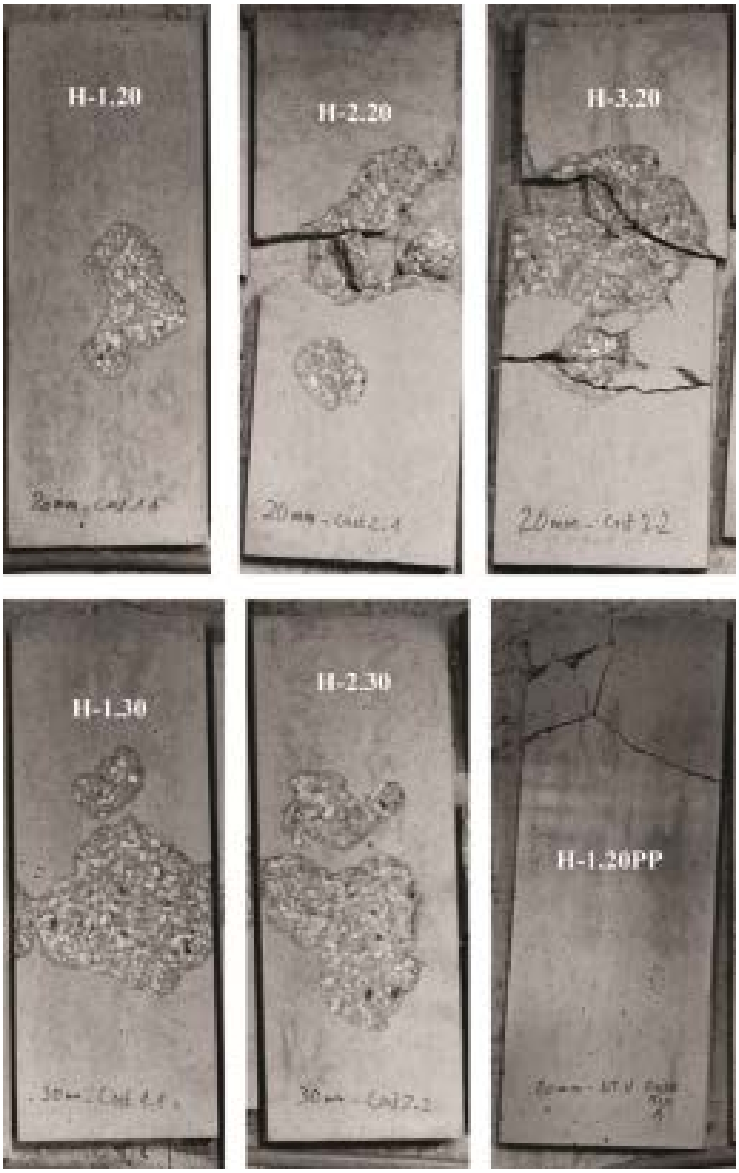

Figure 6 – Spalling types for all H-TRIS specimens except H-20PP.2

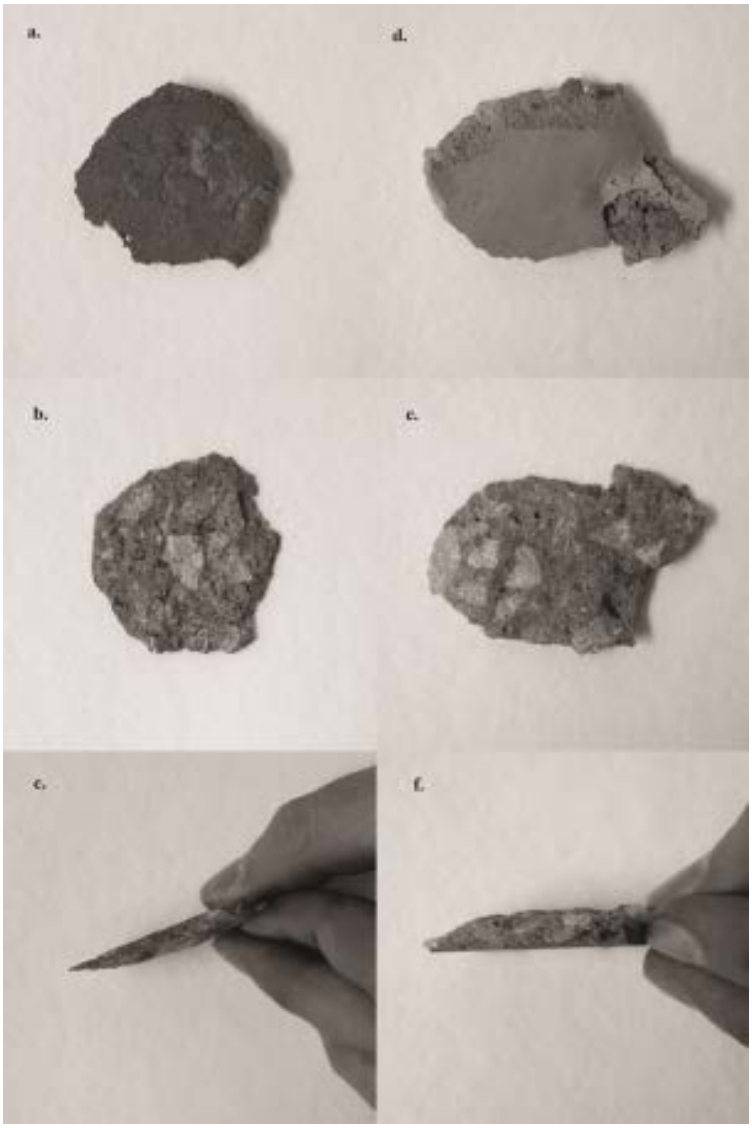

Figure 7 – Debris from H-2.20PP showing that spalling occurred on both sides simultaneously

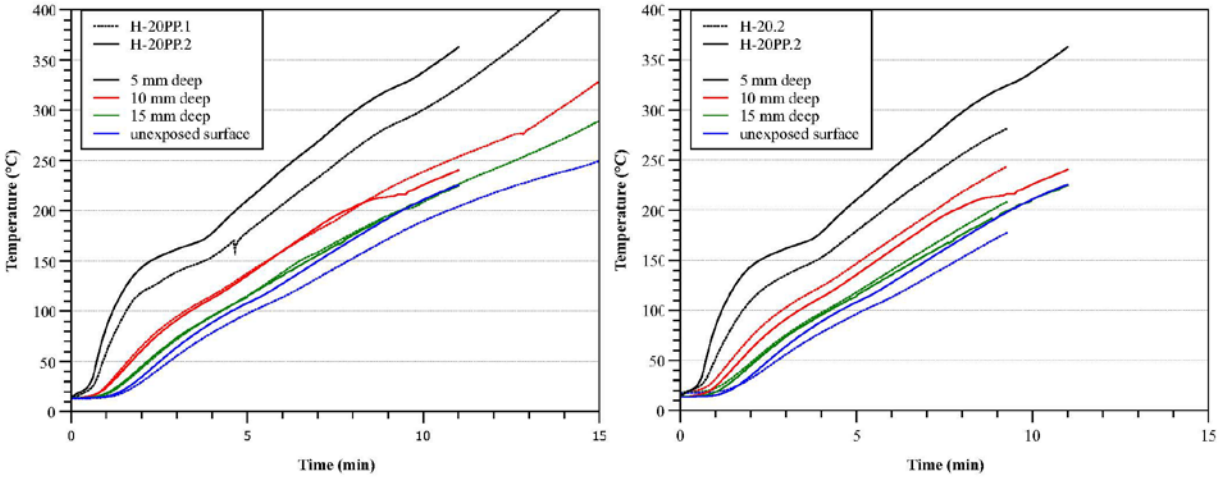

635

636 Figure 8 – Temperature recordings for H-TRIS specimens with HPC PP (left) compared to a
637 specimen with plain HPC (right)

638

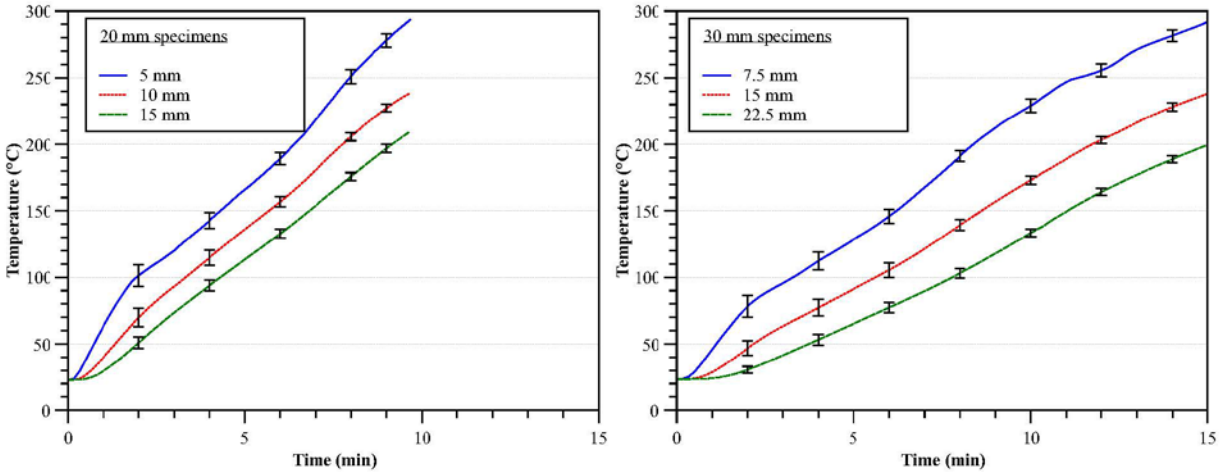

639

640 Figure 9 – Qualitative sensitivity analysis on thermocouple position for a displacement of 1 mm on
641 each side of the originally assumed location